


Localization transitions and winding numbers for non-Hermitian Aubry-André-Harper models with off-diagonal modulations

Xiaoming Cai ^{*}

State Key Laboratory of Magnetic Resonance and Atomic and Molecular Physics, Wuhan Institute of Physics and Mathematics, APM, Chinese Academy of Sciences, Wuhan 430071, China



(Received 21 August 2022; revised 4 November 2022; accepted 8 December 2022; published 23 December 2022)

We study localization and topological properties, as well as the fate of the critical phase, of non-Hermitian generalizations of the Aubry-André-Harper model with both on-site and off-diagonal incommensurate modulations. Non-Hermiticity arises from nonreciprocal hopping and a complex phase in the potential. In the absence of nonreciprocal hopping, we compute analytically the localization length of single-particle states by applying Avila's global theory. The system has the same phase diagram as Hermitian cases, except that the complex phase renormalizes the strength of the potential. In the presence of nonreciprocal hopping, the phase diagram is analytically determined by a similarity transformation. Due to the presence of the skin effect, induced by nonreciprocity, the skin phase turns into extended and critical phases when the boundary condition changes from open to periodic, while states are localized asymmetrically in the boundary-independent localized phase. The nonreciprocal hopping is in favor of the critical phase under a periodic boundary condition. The spectra are complex, and loops always exist. A winding number is not a proper indicator of the presence of loops, but the topological transition is in agreement with the localization transition.

DOI: [10.1103/PhysRevB.106.214207](https://doi.org/10.1103/PhysRevB.106.214207)

I. INTRODUCTION

The Aubry-André-Harper (AAH) model [1,2] is a reliable framework for understanding quantum localization and topological states of matter in one dimension (1D). It originates from the dimension reduction of the two-dimensional quantum Hall system [1,3]. Hence, it inherits the nature of the Chern topological insulator and it supports Thouless pumping [4–6]. When the model is made quasiperiodic, it undergoes a localization phase transition from metal to insulator at a finite strength of quasiperiodic potential [1,3,7]. The relationship between quasiperiodicity and localization has been explored in various generalized AAH models [8–12]. Some exhibit exact mobility edges [13–17], i.e., critical energies separating localized and extended states in the spectrum, while others lack any phase transition [18]. An important model is produced by introducing incommensurate modulations on both the on-site potential and the off-diagonal hopping [19–22]. As one of a dozen exactly solvable AAH models with analytical localization properties, it is the only one supporting a large area of the critical phase due to the interplay of modulations. In the critical phase, states have spatially power-law decays, and they are fractal. The AAH models, including the ones with off-diagonal modulations, have been realized in various artificial systems, such as ultracold atoms [16,23–28] and photonic crystals [4,29].

On the other hand, given the ability to experimentally engineer non-Hermitian Hamiltonians [30–36], there has been growing interest in non-Hermitian physics recently [37,38].

Non-Hermiticity is usually achieved by introducing nonreciprocal hoppings and/or complex potentials. It results in various exotic phenomena, such as parity-time (\mathcal{PT}) symmetry breaking [39,40], non-Hermitian topology [41,42], the skin effect [43,44], and revised bulk-edge correspondence [45–50]. In addition to the Anderson localization in non-Hermitian disordered systems [51–57], non-Hermitian generalizations of the AAH model have also been studied extensively very recently [58–79]. Complex potentials result in the \mathcal{PT} symmetry breaking [62–65,68], butterfly spectra [63,69], topological edge states [58,65–69], mobility edges [79–83], and modified localizations [60,68–74,84]. In particular, a relationship between the localization and topology of the spectrum has been reported [67]. The interplay between nonreciprocal hopping and (quasi)periodicity leads to asymmetrical localization and boundary-dependent topologies and self-dualities [61,69,76,82,84]. Despite intensive activities on AAH models, the localization and topological properties of non-Hermitian generalizations of the important family with both on-site and off-diagonal modulations are largely unexplored [78]. The exact solvability and analytical localization properties have not been studied. More importantly, the fate of the critical phase against non-Hermiticity is not clear yet.

In this paper, we study localization and topological phase transitions, as well as the fate of the critical phase against non-Hermiticity, in generalized AAH models with both on-site and off-diagonal incommensurate modulations. A relative phase between these two modulations is introduced, and the non-Hermiticity arises from the nonreciprocal hopping and the complex phase in the quasiperiodic potential. In the absence of nonreciprocal hopping, we compute analytically the localization length of single-particle states by applying Avila's

*cxmpx@wipm.ac.cn

global theory of one-frequency Schrödinger operators [85]. Based on this, we analyze localization properties and determine phase diagrams for systems with different relative phases. In addition, the fate of the critical phase and the effects of the non-Hermiticity (complex phase) on localization are studied, along with the \mathcal{PT} symmetry breaking (or real-complex transition) and the topology of the spectrum. When the nonreciprocal hopping is introduced, the model suffers from the non-Hermitian skin effect, which results in boundary-dependent localization, real-complex transition, and topological transition of the spectrum. By employing a similarity transformation, the localization is studied analytically, which is spatially asymmetric. Phase diagrams are determined that contain boundary-dependent extended, critical, or skin phases. Other boundary-dependent properties, such as topology and real-complex transition of the spectrum, are studied numerically.

The rest of the paper is organized as follows. In Sec. II, we introduce the generalized AAH model. Section III is devoted to the study of the case in the absence of nonreciprocal hopping. We compute analytically the localization length, and we study localization properties. Along with these, \mathcal{PT} symmetry breaking (or real-complex transition) and the topology of the spectrum are also studied numerically. In Sec. IV, we study analytically the asymmetrical localization induced by nonreciprocal hopping. Boundary-dependent properties, such as critical phase, skin phase, real-complex transition, and topology, are also analyzed. Finally, we conclude our main results and propose experiments in Sec. V.

II. MODEL AND HAMILTONIAN

We consider generalized AAH models, which contain a tunable relative phase between on-site and off-diagonal incommensurate modulations. Non-Hermiticity arises from the nonreciprocal hopping and the complex phase in the on-site potential. These models are described by the following tight-binding Hamiltonian:

$$H = \sum_j [t_j(e^{-\eta}c_j^\dagger c_{j+1} + e^\eta c_{j+1}^\dagger c_j) + V_j c_j^\dagger c_j]. \quad (1)$$

c_j^\dagger (c_j) is the creation (annihilation) operator of a particle at site j . η characterizes the nonreciprocity of hoppings and is the source of the non-Hermitian skin effect [43]. t_j and V_j are the modulated hopping amplitude and on-site complex potential, respectively, which are given by

$$\begin{aligned} t_j &= t + W \cos[2\pi\beta(j + 1/2) + \theta], \\ V_j &= 2V \cos(2\pi\beta j + \theta + \delta + ih). \end{aligned} \quad (2)$$

t is the unmodulated part of the hopping amplitude, and it sets the unit of energy ($t = 1$). W and V denote modulation amplitudes of off-diagonal hopping and on-site potential, respectively. θ is a global phase, which is trivial on the localization, and we will set $\theta = 0$ if not specified. δ is the relative phase between off-diagonal and on-site modulations. In the presence of phases θ and δ , we can set both W and V positive real. β is an irrational number characterizing the quasiperiodicity of modulations. It usually takes the value of the inverse of the golden ratio [$\beta = (\sqrt{5} - 1)/2$], which in practice is

approximated by rational numbers $\beta = F_n/F_{n+1}$, with F_n the n th Fibonacci number. Correspondingly, the total number of lattice sites is $L = F_{n+1}$. Furthermore, the imaginary phase ih characterizes non-Hermiticity of the quasiperiodic potential. The model is \mathcal{PT} -symmetric at least when $\eta = 0$ and $\delta = 0$. The parity operator sends the site index j to $-j$ in Eq. (1), and the time-reversal operator turns i into $-i$ in Eq. (2).

In the Hermitian limit ($\eta = h = 0$), the model reduces to the one studied in Ref. [21], where phase diagrams on localization have been determined by computing bandwidth. Here, we determine phase diagrams of the non-Hermitian extension by analytically computing the localization length, which is also valid in the Hermitian limit. When $\eta = 0$ and $W = 0$, the model reduces to the non-Hermitian one studied in Ref. [67]. It showed that \mathcal{PT} -symmetry breaking, topological phase transition, and localization phase transition happen at the same strength of the quasiperiodic potential. Furthermore, the special case with $\delta = 0$ was numerically studied in Ref. [78], where the discordance of three transitions was observed. Here, for the general model, in addition to the exact solvability, we further focus on the effects of the non-Hermiticity on localization and the critical phase, and we study the topology of the spectrum and \mathcal{PT} symmetry breaking (or real-complex transition of the spectrum). The strategy of our study is that we first concentrate on the case in which non-Hermiticity is only from the imaginary phase ih in the potential, which is the subject of the next section. Then in Sec. IV, we further include the nonreciprocity η , which is the source of the skin effect and leads to boundary-dependent behaviors.

III. LOCALIZATION AND TOPOLOGY IN THE ABSENCE OF NONRECIPROCAL HOPPING ($\eta = 0$)

To study localization in the case when the nonreciprocity is absent, we compute analytically the Lyapunov exponent (LE) (or the inverse of the localization length) of single-particle eigenstates by using Avila's global theory of a one-frequency analytical $SL(2, \mathbb{C})$ cocycle [85]. Given a single-particle state $|\Phi\rangle = \sum_j \phi_j c_j^\dagger |0\rangle$ with eigenenergy E , the Schrödinger equation of amplitudes ϕ_j in transfer matrix form is written as

$$\begin{bmatrix} \phi_{j+1} \\ \phi_j \end{bmatrix} = T_j \begin{bmatrix} \phi_j \\ \phi_{j-1} \end{bmatrix}, \quad T_j = \begin{bmatrix} \frac{E-V_j}{t_j} & -\frac{t_{j-1}}{t_j} \\ 1 & 0 \end{bmatrix}. \quad (3)$$

The LE of the state is computed by

$$\gamma_\varepsilon = \lim_{L \rightarrow \infty} \frac{1}{L} \ln \left\| \prod_{j=1}^L T_j(\theta + i\varepsilon) \right\|,$$

where $\|\cdot\|$ denotes the norm of a matrix. The LE $\gamma_{\varepsilon=0} = 0$ indicates that the state is extended or critical, whereas it is localized when $\gamma_{\varepsilon=0} > 0$. Notice that analytical continuation of the global phase ($\theta \rightarrow \theta + i\varepsilon$) has been performed, which plays a crucial role in Avila's global theory. By factorizing out the unbounded term (t_j^{-1}) in the matrix T_j , we can rewrite the transfer matrix as a commutative product. Then, the LE for the unbounded part can be obtained by turning the product into a summation and then into an integral. As for the LE for the remaining matrix, Avila proved that for transfer matrices in the family of one-frequency analytical $SL(2, \mathbb{C})$ cocycles, the

LE $\gamma_{\varepsilon=0}$ can be obtained from $\gamma_{\varepsilon \rightarrow \infty}$. Given that in the limit $\varepsilon \rightarrow \infty$ the norm of the transfer matrix is site-independent, the LE $\gamma_{\varepsilon \rightarrow \infty}$ can be easily computed. Including two parts, we obtain the LE (see the Appendix for details)

$$\gamma = \begin{cases} \max(f_1, 0), & W \leq t, \\ \max(f_2, 0), & W > t, \end{cases} \quad (4)$$

where

$$f_1 = \max \left\{ \ln \frac{|Ve^{\pm(i\delta+h)} + (-)\sqrt{[Ve^{\pm(i\delta+h)}]^2 - W^2}|}{t + \sqrt{t^2 - W^2}} \right\},$$

$$f_2 = \max \left\{ \ln \frac{|Ve^{\pm(i\delta+h)} + (-)\sqrt{[Ve^{\pm(i\delta+h)}]^2 - W^2}|}{W} \right\}.$$

The LE is an even function of h . Furthermore, quantities $f_{1,2}$ and then the LE are periodic functions of the relative phase δ with a period π , and they are also symmetric with respect to $\delta = m\pi/2$, $m \in \mathbb{Z}$. Thus, we can restrict $\delta \in [0, \pi/2]$. Then, when $\delta \in [0, \pi/2]$, $f_{1,2}$ can be simplified to

$$f_1 = \ln \frac{|Ve^{i\delta+|h|} + \sqrt{[Ve^{i\delta+|h|}]^2 - W^2}|}{t + \sqrt{t^2 - W^2}},$$

$$f_2 = \ln \frac{|Ve^{i\delta+|h|} + \sqrt{[Ve^{i\delta+|h|}]^2 - W^2}|}{W}, \quad (5)$$

by analyzing the magnitudes of the complex numerators above. Localization phase transition points are determined by conditions $f_{1(2)} = 0$, which indicate that the state changes from extended or critical to localized, or the LE changes from $\gamma = 0$ to $\gamma > 0$. $f_1 = 0$ leads to

$$Ve^{|h|}/t = \sqrt{\frac{t^2 - W^2}{t^2 - W^2 \cos^2 \delta}} \quad \text{when } W \leq t, \quad (6)$$

while $f_2 = 0$ results in

$$Ve^{|h|} = \begin{cases} W & \text{if } \delta = 0, \\ 0 & \text{if } \delta \neq 0, \end{cases} \quad \text{when } W > t. \quad (7)$$

It is worth noticing that $f_2 = 0$ holds in a large area of the parameter space, which indicates the presence of the critical phase. The LE and conditions for phase transition are energy-independent. Thus, there is no mobility edge. They are also independent of the irrational frequency β and global phase θ . Furthermore, note that in the exact expressions of the LE and conditions for phase transition, the imaginary phase ih only renormalizes the strength V by $e^{|h|}$. Other than these, the localization is the same as for the Hermitian model ($h = 0$).

On the other hand, due to its complex nature, the energy spectrum of a non-Hermitian system can have nontrivial topological structures (loops) [41,44,46,48,49,59,67,84]. To study the topology of the spectrum, the winding number is introduced, which is defined by [41,59,67,84]

$$\nu_{E_B} = \lim_{L \rightarrow \infty} \frac{1}{2\pi i} \int_0^{2\pi/L} d\theta \frac{\partial}{\partial \theta} \ln[\det(H - E_B)]. \quad (8)$$

It characterizes how the complex spectral trajectory E encircles a base energy E_B in the complex energy plane, when θ changes from 0 to 2π . Similar to the case in the Non-Bloch band theory [41], the imaginary phase ih complexifies the

artificial ‘‘momentum’’ θ and results in nontrivial winding numbers. In other words, ν_{E_B} characterizes the topology of the spectrum induced by h . Different choices of the base energy E_B give winding numbers characterizing different loop structures. We concentrate on the most nontrivial winding number for any E_B , i.e., $\nu = \text{sgn}(\nu_{E_B}) \times \max(|\nu_{E_B}|)$, $\forall E_B \in \mathbb{C}$, which is usually used to characterize the existence of loops in the complex energy plane [59,67,84].

A. Case $\delta = 0$

From Eqs. (6) and (7), one can clearly see the particularity of the case $\delta = 0$. Simplified from them, localization transition points are determined by the condition

$$Ve^{|h|} = \max(t, W). \quad (9)$$

When $Ve^{|h|} > \max(t, W)$, the system is in the localized phase, where all single-particle states are localized with energy-independent LEs $\gamma > 0$. But $f_1 < 0$, $\gamma = 0$, all states are extended, and the system is in the extended phase, when $Ve^{|h|} < t$ and $W < t$. When $Ve^{|h|} < W$ and $W > t$, we have $f_2 = 0$ and $\gamma = 0$, and the system is in the critical phase where all states are critical. Furthermore, in the localized phase, by expanding the LE around phase transition points, we have $\gamma \propto |Ve^{|h|}/t - 1|^1$ when $W < t$. The critical exponent 1 is the same as that for the classic AAH model, indicating they are in the same universality class. However, when $W > t$, we obtain $\gamma \propto |Ve^{|h|}/W - 1|^{1/2}$ and the system belongs to a different and unusual universality class. The critical exponent 1/2 was recently reported in a generalized AAH model with unbounded potentials [86].

The above analytical results are consistent with numerical simulations. We adopt exponential wave functions $\phi_j^n = \exp(-\gamma_n |j - j_0|)$, with j_0 the localization center, n the index of states, and γ_n the LE. Extracted by fitting numerical single-particle eigenstates with the above wave functions, the mean LEs $\gamma = \sum_n \gamma_n / L$ versus V for systems with different h are shown in the inset of Fig. 1(a). From hereon, the averaging is performed over all eigenstates, with n the index. After rescaling ($V \rightarrow Ve^{|h|}$), all curves collapse into a single one and agree well with the theoretical prediction in Eq. (4) [see Fig. 1(a)]. Besides, we also calculate the inverse of the participation ratios (IPRs) and fractal dimensions of single-particle states. For a normalized state, the IPR is defined by $P = \sum_j |\phi_j|^4$. In general, the IPR $P \propto L^{-\alpha}$ with α the fractal dimension. For an extended state, $P \propto 1/L$ and $\alpha = 1$, whereas the IPR approaches 1 and $\alpha = 0$ for a localized state. States with $0 < \alpha < 1$ are critical and have multifractal properties. In Fig. 1(b), we present a mean fractal dimension $\text{MFD} = \sum_n \alpha_n / L$ in the $(Ve^{|h|}, W)$ plane, which is numerically extracted by the box-counting method [84]. The boundary between localized and extended (critical) phases is precisely described by Eq. (9), and the black dashed-dotted line corresponds to $W = t$, separating extended and critical phases. After the rescaling, the phase diagrams are the same for systems with different h , including the Hermitian one [21].

In addition to localization of states, we also study the properties of the spectrum. In Fig. 1(c) we show an example of how the spectrum changes as V increases. The real-complex transition (or \mathcal{PT} symmetry breaking) most likely happens

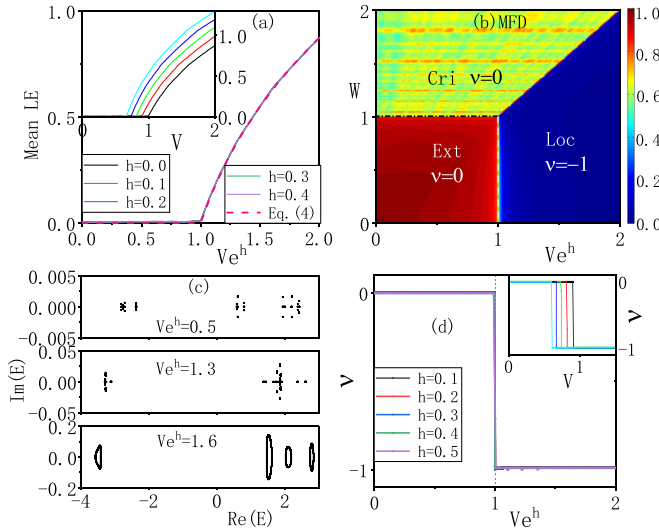


FIG. 1. Generalized AAH model in the absence of nonreciprocal hopping ($\eta = 0$) and with relative phase $\delta = 0$. In (a) and its inset we present mean LEs vs Ve^h and V , respectively, for systems with $W = 0.8$. (b) Mean fractal dimension in the (Ve^h, W) plane for the system with $h = 0.2$. (c) Spectra in the complex energy plane for systems with $W = 1.5$ and $h = 0.2$. In (d) and its inset we show winding numbers vs Ve^h and V , respectively, for systems with $W = 0.5$. The size of the lattice is $L = 610$.

at $V = 0$, since as V increases there is no sharp increase in the largest value of $\log_{10} |\text{Im}(E)|$. The sharp increase is a characteristic signature of the transition [87]. Moreover, there are loops in the spectrum when the system is in the localized phase, while they are absent in the extended and critical phases. To characterize the presence of loops, we present winding numbers versus V in the inset of Fig. 1(d), which are numerically calculated by Eq. (8). After the rescaling, they all collapse into one curve [Fig. 1(d)]. The topological phase transition point is the same as the localization one (dot line). Winding numbers in different phases are shown in Fig. 1(b).

B. Case $\delta = \pi/2$

When $\delta = \pi/2$, the condition for the localization phase transition reduces to

$$\begin{aligned} Ve^{|h|} &= \sqrt{t^2 - W^2} & \text{if } W \leq t, \\ V &= 0 & \text{if } W > t. \end{aligned} \quad (10)$$

Except for the renormalization of V by $e^{|h|}$, the localization is still the same as for the Hermitian model. In Fig. 2(a) we present numerical mean LEs, which agree well with and validate the theoretical prediction in Eq. (4). Besides, in Fig. 2(b) we show the mean inverse of the participation ratio, $\text{MIPR} = \sum_n P_n/L$, in the (Ve^h, W) plane. When $Ve^{|h|} < \sqrt{t^2 - W^2}$ and $W < t$, the system is in the extended phase, $\text{MIPR} \propto 1/L$, mean fractal dimension $\text{MFD} \simeq 1$, and LEs $\gamma = 0$. Elsewhere, except when $W > t$ and $V = 0$, the system is in the localized phase, MIPR approaches 1, $\text{MFD} \simeq 0$, and LEs $\gamma > 0$. Critical states only exist at the boundary between phases or when $W > t$ and $V = 0$, which are in agreement with Eqs. (10).

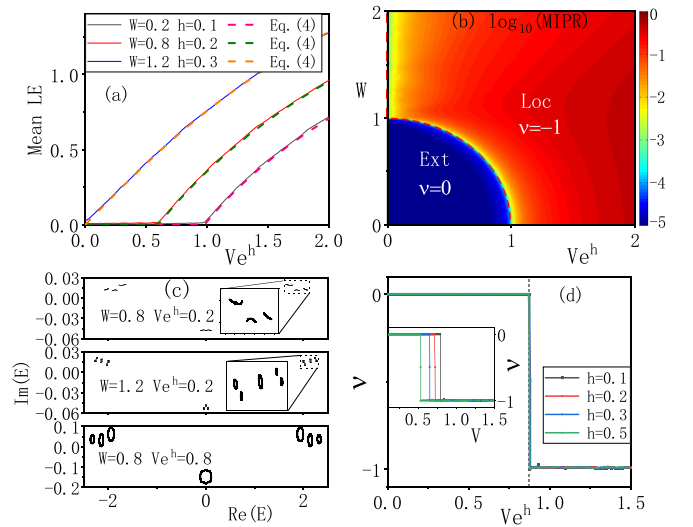


FIG. 2. Generalized AAH model in the absence of nonreciprocal hopping ($\eta = 0$) and with $\delta = \pi/2$. (a) Mean LEs vs Ve^h for systems with different W and h . (b) The quantity $\log_{10}(\text{MIPR})$ in the (Ve^h, W) plane for the system with $h = 0.2$. (c) Spectra of systems with $h = 0.2$. In (d) and its inset we present winding numbers vs Ve^h and V , respectively, for systems with $W = 0.5$. The size of the lattice is $L = 610$.

We present typical spectra in Fig. 2(c). The spectrum of the system is complex, as long as $V > 0$, $W > 0$, and $h \neq 0$. Moreover, there is no loop when the system is in the extended phase, while there are when in the localized phase. We present winding numbers versus Ve^h (V) in (the inset of) Fig. 2(d), where the topological phase transition point is the same as the localization one (dot line). Winding numbers in different phases are also shown in Fig. 2(b).

With a general δ , the system has similar localization and topological properties as in the case $\delta = \pi/2$. Numerical mean LEs still agree with the theoretical prediction in Eq. (4), and the rescaling and collapse still hold (not shown). In Fig. 3,

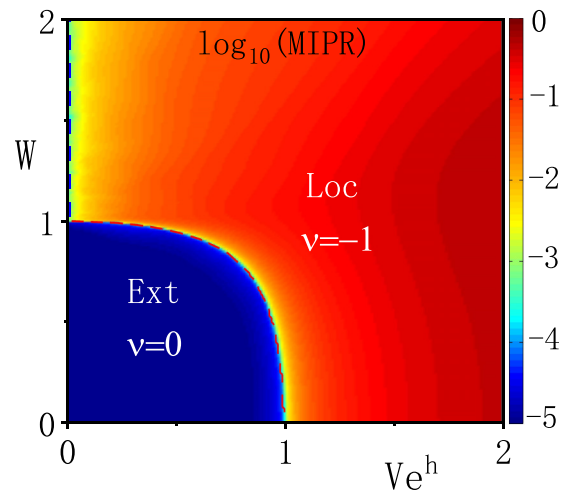


FIG. 3. The quantity $\log_{10}(\text{MIPR})$ of the generalized AAH model in the absence of nonreciprocal hopping ($\eta = 0$), and with $\delta = \pi/5$, $h = 0.2$, and $L = 610$.

we present a typical mean inverse of the participation ratio in the (Ve^{ih}, W) plane, which has the same structure as the one for $\delta = \pi/2$. Dotted lines, describing phase boundaries that are different from the ones for $\delta = \pi/2$, correspond to Eqs. (6) and (7). The spectrum of the non-Hermitian system is still complex. There are loops in the spectrum when the system is in the localized phase; otherwise, there are not. Corresponding winding numbers are shown in Fig. 3, and the topological transition point is still the same as the localization one.

IV. ASYMMETRICAL LOCALIZATION IN THE PRESENCE OF NONRECIPROCAL HOPPING ($\eta \neq 0$)

In the presence of nonreciprocal hopping, the model supports the non-Hermitian skin effect and it has a boundary-dependent spectrum and states. We first concentrate on the case under open boundary condition (OBC). Analytical localization properties can be explored by employing a similarity transformation. Under OBC, the Hamiltonian in Eq. (1) can be mapped to

$$H_1 = \sum_j [t_j(\tilde{a}_j a_{j+1} + \tilde{a}_{j+1} a_j) + V_j \tilde{a}_j a_j] \quad (11)$$

by the asymmetric similarity transformation $c_j = e^{\eta j} a_j$ and $c_j^\dagger = e^{-\eta j} \tilde{a}_j$. a_j (\tilde{a}_j) is the annihilation (creation) operator of a particle. $[a_j, \tilde{a}_{j'}]_{\pm} = \delta_{jj'}$, but \tilde{a}_j is not the Hermitian

conjugate of a_j due to the non-Hermiticity of the system. The Hamiltonian H_1 has the same single-particle physics as the Hamiltonian $H(\eta = 0)$, in which the nonreciprocal hopping is absent. Related by the transformation, Hamiltonians H and $H(\eta = 0)$ have exactly the same spectra and winding numbers under OBC.

As for the single-particle states, a correspondence can be made. Given that ϕ_j^n is a right eigenstate of H_1 , $\varphi_j^n = e^{\eta j} \phi_j^n$ is an eigenstate of H . This clearly shows how the nonreciprocal hopping affects states in different phases: for extended and critical eigenstates of H_1 , corresponding wave functions φ_j^n are localized at the right end with left side LEs $\gamma^L = |\eta|$ when $\eta > 0$, or at the left end with right side LEs $\gamma^R = |\eta|$ when $\eta < 0$; for localized eigenstates of H_1 , wave functions φ_j^n have the form

$$\varphi_j^n \propto \begin{cases} e^{-(\gamma-\eta)(j-j_0)}, & j > j_0, \\ e^{-(\gamma+\eta)(j_0-j)}, & j < j_0, \end{cases} \quad (12)$$

where γ was given in Eq. (4). Thus, in the localized phase, the right and left side LEs are $\gamma^R = \gamma - \eta$ and $\gamma^L = \gamma + \eta$, respectively. Apparently, under OBC, states are asymmetrically localized due to the presence of nonreciprocal hopping. The condition $\gamma - |\eta| > 0$ indicates bulk localization of all eigenstates, while $\gamma - |\eta| < 0$ implies that the system is in the skin phase where all eigenstates are located at the edge. The condition $\gamma - |\eta| = 0$ determines phase transition points. Putting Eqs. (4) and (5) in, we obtain the condition for localization phase transition,

$$[Ve^{|\eta|}]^2 \left[\frac{\cos^2 \delta}{(t \cosh |\eta| + \sqrt{t^2 - W^2} \sinh |\eta|)^2} + \frac{\sin^2 \delta}{(t \sinh |\eta| + \sqrt{t^2 - W^2} \cosh |\eta|)^2} \right] = 1 \quad \text{when } W \leq t, \\ \left[\frac{Ve^{|\eta|}}{W} \right]^2 \left[\frac{\cos^2 \delta}{\cosh^2 |\eta|} + \frac{\sin^2 \delta}{\sinh^2 |\eta|} \right] = 1 \quad \text{when } W > t. \quad (13)$$

A. Case $\delta = 0$

When $\delta = 0$, the condition for the phase transition in Eqs. (13) reduces to

$$Ve^{|\eta|} = t \cosh |\eta| + \sqrt{t^2 - W^2} \sinh |\eta| \quad \text{if } W \leq t, \\ Ve^{|\eta|} = W \cosh |\eta| \quad \text{if } W > t. \quad (14)$$

The above analytical results for systems under OBC are consistent with numerical simulations. In Fig. 4(a) and its inset we show numerical mean left and right side LEs versus Ve^{ih} , respectively. The imaginary phase ih in the potential still renormalizes V by $e^{|\eta|}$, and the rescaling and collapse still hold, regardless of the value of relative phase δ (not shown). When $Ve^{|\eta|}$ is small, the system is in the skin phase [59,76], where all states are localized at one edge. Here, for a positive η , states are localized at the right edge, $\gamma^L = \eta$, and γ^R is undefined. When $Ve^{|\eta|}$ is large enough, the system is in the localized phase, states are asymmetrically localized in the bulk, and $\gamma^L = \gamma^R + 2\eta$. States in both skin and localized phases are localized, but with different localization details. Transition points are determined by Eqs. (14) (dot lines), where γ^L expe-

rience a sudden jump of size 2η . Just before the transition, the system is still in the skin phase but with a decreasing γ^L , and delocalization of states happens. The delocalization proceeds from the transition point of the corresponding system with $\eta = 0$ [Eqs. (9) and dashed-dotted lines in Fig. 4(a)] to the transition point of the system with finite η [Eqs. (14) and dashed lines in Fig. 4(a)]. Besides LEs, in Fig. 4(b) we further show $\log_{10}(\text{MIPR})$ in the $(Ve^{|\eta|}, W)$ plane. The mean inverse of the participation ratios approaches 1 in both the skin and localized phases. Phase transition points correspond to the most extended cases with the smallest MIPR, which agree with the condition in Eqs. (14) (dashed lines).

Under the periodic boundary condition (PBC), the similarity transformation does not work, and systems have different properties of states and spectra. In Fig. 4(c) we present the mean fractal dimension of states in the (Ve^{ih}, W) plane. The renormalization effect of ih still holds. When $Ve^{|\eta|}$ is small, the system is in the extended phase with MFD $\simeq 1$ if $W < t$, and in the critical phase with $0 < \text{MFD} < 1$ if $W > t$, which both turn into the skin phase when under OBC. The system is in the localized phase for a large enough $Ve^{|\eta|}$. Given that

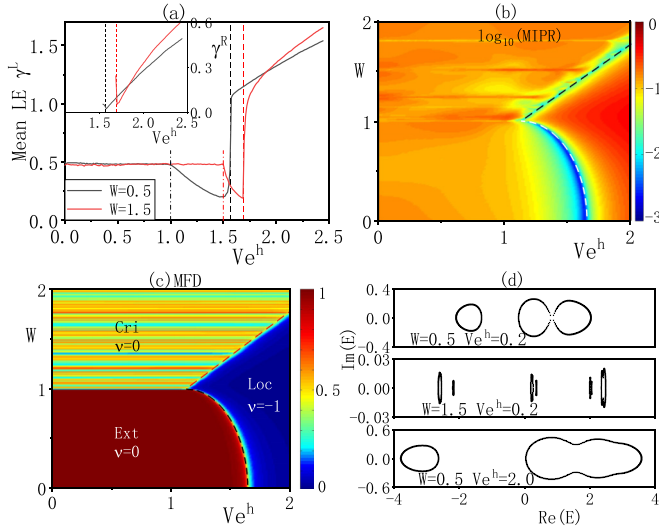


FIG. 4. Generalized AAH model in the presence of nonreciprocal hopping ($\eta = 0.5$) and with $\delta = 0$. In (a) and its inset, we show mean left and right side LEs vs Ve^h , respectively. (b) The quantity $\log_{10}(\text{MIPR})$ in the (Ve^h, W) plane. In (a) and (b), OBC is used, the lattice size is $L = 233$, and $h = 0.2$. (c) Mean fractal dimension in the (Ve^h, W) plane. (d) Typical spectra. In (c) and (d), PBC is used, the lattice size is $L = 610$, and $h = 0.2$. Dashed lines correspond to Eqs. (14), and dashed-dotted ones correspond to Eq. (9).

localized states in the bulk should be independent of boundary conditions, localization details in the localized phase are the same when under different boundary conditions, and phase transition points are still described by Eqs. (14) (dashed lines). The region of critical phase is enlarged due to the presence of nonreciprocal hopping [see Figs. 1(b) and 4(c)]. In addition, in Fig. 4(c) we also show winding numbers of spectra for systems under PBC. The topological phase transition point is the same as the localization one, while it is not the same in the case when under OBC [see Figs. 1(b) and 4(b)]. Furthermore, the winding number is no longer an indicator of the presence of loops in the spectrum when both η and h are finite. In Fig. 4(d) we present typical spectra in different phases for systems under PBC. Loops always exist except at the phase transition points, but winding numbers are zero in both extended and critical phases. The topology of the spectrum can originate from the nonreciprocity η , which the winding number ν cannot characterize. The spectrum of the system is complex as long as the model is non-Hermitian.

B. Case $\delta = \pi/2$

When $\delta = \pi/2$, phase transition points are determined by the condition

$$\begin{aligned} Ve^{|h|} &= t \sinh |\eta| + \sqrt{t^2 - W^2} \cosh |\eta| \quad \text{if } W \leq t, \\ Ve^{|h|} &= W \sinh |\eta| \quad \text{if } W > t. \end{aligned} \quad (15)$$

In Fig. 5(a) and its inset, we present numerical mean left and right side LEs versus Ve^h , respectively, for systems under OBC. Similar to the case $\delta = 0$, the system is in the skin phase when $Ve^{|h|}$ is small, while it is in the asymmetrically localized phase for a large enough $Ve^{|h|}$, and $\gamma^L = \gamma^R + 2\eta$.

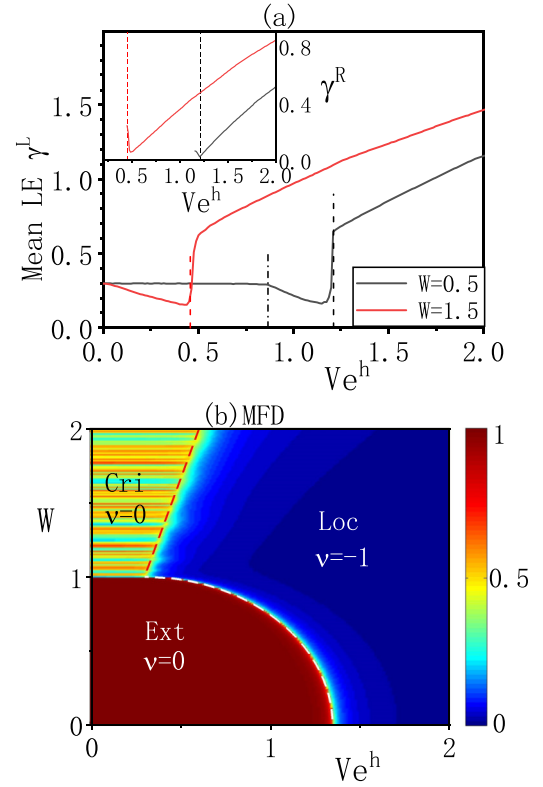


FIG. 5. Generalized AAH model in the presence of nonreciprocal hopping ($\eta = 0.3$) and with $\delta = \pi/2$. In (a) and its inset, we present mean left and right side LEs vs Ve^h , respectively, for systems under OBC and with $h = 0.2$ and $L = 233$. (b) Mean fractal dimension of the system under PBC and with $h = 0.2$ and $L = 610$.

Transition points are described by Eqs. (15) (dash lines), where there exists a sudden jump of 2η for γ^L . The delocalization of states still proceeds between the above-mentioned two phase transition points [Eqs. (10) and (15), and dashed (dotted) lines in Fig. 5(a)]. But here, the system in the skin phase is always delocalizing when $W > t$, since the transition point is at $V = 0$ when $\eta = 0$. On the other hand, due to the boundary-dependent nature, in Fig. 5(b) we show the mean fractal dimension in the (Ve^h, W) plane for a system under PBC. Since localized bulk states are independent of boundary conditions, localization properties in the localized phase and transition points are the same for systems under OBC and PBC. However, before the transition, things are different. Under PBC, the nonreciprocal hopping leads to a critical phase when $W > t$, while the system is in the extended phase when $W < t$. The stronger the nonreciprocity η is, the larger is the region of the critical phase, which is absent when $\eta = 0$. Both phases turn into the skin phase when the boundary condition changes into OBC. Winding numbers of spectra for systems in different phases are also shown in Fig. 5(b), and the topological phase transition is in agreement with the localization one. Loops always exist in spectra except at the phase transition points, and spectra are complex when η , h , and V are finite.

With a general δ , the system has similar localization and topological properties to those in the case $\delta = \pi/2$. In Fig. 6, we show a typical mean fractal dimension of a system under PBC, along with winding numbers of spectra in different

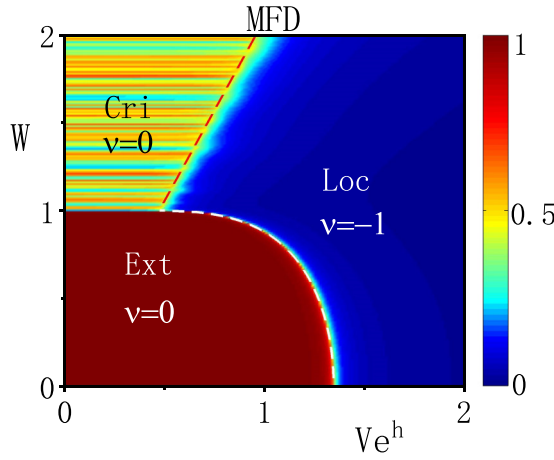


FIG. 6. Mean fractal dimension of the generalized AAH model in the presence of nonreciprocal hopping ($\eta = 0.3$), and with $\delta = \pi/5$, $h = 0.2$, and $L = 610$. PBC is used.

phases. Phase boundaries are determined by Eqs. (13) (dashed line). Under PBC, the nonreciprocal hopping is in favor of the critical phase when $W > t$. Both extended and critical phases turn into the skin phase when PBC changes into OBC. When $W > t$ the system in the skin phase is always delocalizing. The spectrum is complex and loops always exist.

V. CONCLUSION AND DISCUSSION

We have studied localization and topological properties of generalized AAH models with both on-site and off-diagonal modulations. A relative phase between two modulations is introduced, and its effects have been thoroughly studied. Non-Hermiticity arises from the nonreciprocal hopping and the complex phase in the potential. Applying Avila's global theory, we first analytically computed the LE of single-particle states for systems in the absence of nonreciprocal hopping, which is also valid in the Hermitian case. Based on that, we analyzed localization properties and determined phase diagrams. The localization is the same as in the Hermitian case, except that the complex phase renormalizes the strength of the potential. The same renormalization effect was observed in a non-Hermitian model with only on-site modulation [67]. When the off-diagonal modulation is strong enough, the model is in a different universality class from the one for the classic AAH model. Topological phase transition is in agreement with the localization one. Winding numbers correctly characterize the presence of loops in spectra. The spectrum of the system is complex as long as the model is non-Hermitian.

In the presence of nonreciprocal hopping, the model supports the skin effect and has a boundary-dependent spectrum and states. Under OBC, localization properties of systems can be analytically studied by employing a similarity transformation, and phase diagrams are precisely determined. The system turns from the skin phase into the asymmetrically localized phase as the strength of the potential increases. When the boundary condition changes from open to periodic, the skin phase turns into the extended and critical phases, while the localized phase does not change. Nonreciprocal hopping is in favor of the critical phase when under PBC. Loops always exist in spectra, and spectra are complex. The topological

phase transition is still in agreement with the localization one, but the winding number is no longer a proper indicator of the presence of loops in the spectrum.

The single-particle physics studied above can be experimentally tested in electric circuits [74], which recently have turned out to be powerful platforms to simulate non-Hermitian and/or topological phases [38]. The eigenvalue problem is simulated by Kirchhoff's current law $I_a = \sum_{b=1}^L J_{ab} V_b$, where the Laplacian of circuit J acts as the effective Hamiltonian, and I_a and V_a are the current and voltage at node a . On-site complex potentials are provided by grounding nodes with proper resistors [88], and nonreciprocal hoppings are realized by negative impedance converters with current inversion (IN-ICs) [89]. Furthermore, the boundary-dependent spectra could be obtained by measuring two-node impedances [69].

ACKNOWLEDGMENTS

This work is supported by the National Natural Science Foundation of China under Grants No. 12134015 and No. 12175290.

APPENDIX: COMPUTATION OF THE LYAPUNOV EXPONENT

Factorizing out the unbounded term, we rewrite the transfer matrix in Eq. (3) as

$$T_j = \begin{bmatrix} \frac{E-V_j}{t_j} & -\frac{t_{j-1}}{t_j} \\ 1 & 0 \end{bmatrix} = A_j B_j, \quad (\text{A1})$$

where

$$A_j = \frac{1}{t + W \cos[2\pi\beta(j+1/2) + \theta]},$$

$$B_j = \begin{bmatrix} E - V_j & -t_{j-1} \\ t_j & 0 \end{bmatrix}. \quad (\text{A2})$$

t_j and V_j are the modulated off-diagonal hopping and on-site complex potential, respectively [Eqs. (2)]. The LE of the single-particle state is computed by

$$\begin{aligned} \gamma(E) &= \lim_{L \rightarrow \infty} \frac{1}{L} \ln \left\| \prod_{j=1}^L T_j \right\| \\ &= \lim_{L \rightarrow \infty} \frac{1}{L} \ln \left\| \prod_{j=1}^L A_j \right\| + \lim_{L \rightarrow \infty} \frac{1}{L} \ln \left\| \prod_{j=1}^L B_j \right\| \\ &= \gamma^A(E) + \gamma^B(E), \end{aligned} \quad (\text{A3})$$

where $\|\cdot\|$ denotes the norm of a matrix, which is defined by the largest absolute value of its eigenvalues. Applying ergodic theory [90] and Jensen's formula [91], we obtain

$$\begin{aligned} \gamma^A(E) &= \lim_{L \rightarrow \infty} \frac{1}{L} \ln \prod_{j=1}^L \frac{1}{|t + W \cos[2\pi\beta(j+1/2) + \theta]|} \\ &= \frac{1}{2\pi} \int_0^{2\pi} \ln \frac{1}{|t + W \cos\theta|} d\theta \\ &= \begin{cases} \ln \frac{2}{t + \sqrt{t^2 - W^2}}, & W \leq t, \\ \ln \frac{2}{W}, & W > t. \end{cases} \end{aligned} \quad (\text{A4})$$

To compute $\gamma^B(E)$, we employ Avila's global theory. The first step in the computation is to carry out an analytical continuation of the global phase, i.e., $\theta \rightarrow \theta + i\varepsilon$. In the absence of ambiguity, we will use the same symbol for a quantity and its analytical continuation. In the limit $\varepsilon \rightarrow +\infty$, a direct computation yields

$$B_j(\varepsilon \rightarrow +\infty) = e^{-i2\pi\beta j + \varepsilon} \begin{bmatrix} -Ve^{-i\delta+h} & -We^{i\pi\beta}/2 \\ We^{-i\pi\beta}/2 & 0 \end{bmatrix} + o(1), \quad (\text{A5})$$

which leads to

$$\gamma_{\varepsilon \rightarrow +\infty}^B(E) = \varepsilon + \max \left\{ \ln \frac{|Ve^{i\delta+h} \pm \sqrt{[Ve^{i\delta+h}]^2 - W^2}|}{2} \right\}. \quad (\text{A6})$$

On the other side, in the limit $\varepsilon \rightarrow -\infty$, we obtain

$$B_j(\varepsilon \rightarrow -\infty) = e^{i2\pi\beta j - \varepsilon} \begin{bmatrix} -Ve^{i\delta-h} & -We^{-i\pi\beta}/2 \\ We^{i\pi\beta}/2 & 0 \end{bmatrix} + o(1), \quad (\text{A7})$$

and the corresponding LE is

$$\gamma_{\varepsilon \rightarrow -\infty}^B(E) = |\varepsilon| + \max \left\{ \ln \frac{|Ve^{-(i\delta+h)} \pm \sqrt{[Ve^{-(i\delta+h)}]^2 - W^2}|}{2} \right\}. \quad (\text{A8})$$

According to Avila's global theory, as a function of ε , $\gamma_\varepsilon^B(E)$ is a convex, piecewise linear function with integer slopes. Moreover, the theory shows that the energy E does not belong to the spectrum if and only if $\gamma_{\varepsilon=0}^B(E) > 0$, and $\gamma_\varepsilon^B(E)$ is an affine function in the neighborhood of $\varepsilon = 0$. Including $\gamma^A(E)$, we obtain the LE of the single-particle state,

$$\gamma(E) = \begin{cases} \max \left(f + \ln \frac{2}{t + \sqrt{t^2 - W^2}}, 0 \right), & W \leq t, \\ \max \left(f + \ln \frac{2}{W}, 0 \right), & W > t, \end{cases} \quad (\text{A9})$$

where

$$f = \max \left\{ \begin{array}{l} \ln \frac{|Ve^{i\delta+h} + \sqrt{[Ve^{i\delta+h}]^2 - W^2}|}{2} \\ \ln \frac{|Ve^{i\delta+h} - \sqrt{[Ve^{i\delta+h}]^2 - W^2}|}{2} \\ \ln \frac{|Ve^{-i\delta-h} + \sqrt{[Ve^{-i\delta-h}]^2 - W^2}|}{2} \\ \ln \frac{|Ve^{-i\delta-h} - \sqrt{[Ve^{-i\delta-h}]^2 - W^2}|}{2} \end{array} \right\}. \quad (\text{A10})$$

-
- [1] S. Aubry and G. André, *Ann. Israel. Phys. Soc.* **3**, 133 (1980).
[2] P. G. Harper, *Proc. Phys. Soc. A* **68**, 874 (1955).
[3] D. R. Hofstadter, *Phys. Rev. B* **14**, 2239 (1976).
[4] Y. E. Kraus, Y. Lahini, Z. Ringel, M. Verbin, and O. Zeitler, *Phys. Rev. Lett.* **109**, 106402 (2012).
[5] L. J. Lang, X. Cai, and S. Chen, *Phys. Rev. Lett.* **108**, 220401 (2012).
[6] S. Ganeshan, K. Sun, and S. Das Sarma, *Phys. Rev. Lett.* **110**, 180403 (2013).
[7] S. Y. Jitomirskaya, *Ann. Math.* **150**, 1159 (1999).
[8] S. Das Sarma, S. He, and X. C. Xie, *Phys. Rev. Lett.* **61**, 2144 (1988).
[9] X. Cai, L. J. Lang, S. Chen, and Y. Wang, *Phys. Rev. Lett.* **110**, 176403 (2013).
[10] M. Rossignolo and L. Dell'Anna, *Phys. Rev. B* **99**, 054211 (2019).
[11] X. Deng, S. Ray, S. Sinha, G. V. Shlyapnikov, and L. Santos, *Phys. Rev. Lett.* **123**, 025301 (2019).
[12] S. Roy, T. Mishra, B. Tanatar, and S. Basu, *Phys. Rev. Lett.* **126**, 106803 (2021).
[13] Y. Wang, X. Xia, L. Zhang, H. Yao, S. Chen, J. You, Q. Zhou, and X.-J. Liu, *Phys. Rev. Lett.* **125**, 196604 (2020).
[14] J. Biddle and S. Das Sarma, *Phys. Rev. Lett.* **104**, 070601 (2010).
[15] S. Ganeshan, J. H. Pixley and S. Das Sarma, *Phys. Rev. Lett.* **114**, 146601 (2015).
[16] F. A. An, K. Padavić, E. J. Meier, S. Hegde, S. Ganeshan, J. H. Pixley, S. Vishveshwara, and B. Gadway, *Phys. Rev. Lett.* **126**, 040603 (2021).
[17] T. Liu, S. Cheng, R. Zhang, R. Ruan, and H. Jiang, *Chin. Phys. B* **31**, 027101 (2022).
[18] D. R. Grempel, S. Fishman, and R. E. Prange, *Phys. Rev. Lett.* **49**, 833 (1982).
[19] D. J. Thouless, *Phys. Rev. B* **28**, 4272 (1983).
[20] I. Chang, K. Ikezawa, and M. Kohmoto, *Phys. Rev. B* **55**, 12971 (1997).
[21] F. Liu, S. Ghosh, and Y. D. Chong, *Phys. Rev. B* **91**, 014108 (2015).
[22] Y. Wang, C. Cheng, X.-J. Liu, and D. Yu, *Phys. Rev. Lett.* **126**, 080602 (2021).
[23] G. Roati, C. D'Errico, L. Fallani, M. Fattori, C. Fort, M. Zaccanti, G. Modugno, M. Modugno, and M. Inguscio, *Nature (London)* **453**, 895 (2008).
[24] X. Li, X. Li, and S. Das Sarma, *Phys. Rev. B* **96**, 085119 (2017).
[25] H. P. Lüschen, S. Scherg, T. Kohlert, M. Schreiber, P. Bordia, X. Li, S. Das Sarma, and I. Bloch, *Phys. Rev. Lett.* **120**, 160404 (2018).
[26] T. Kohlert, S. Scherg, X. Li, H. P. Lüschen, S. Das Sarma, I. Bloch, and M. Aidelsburger, *Phys. Rev. Lett.* **122**, 170403 (2019).
[27] V. Goblot, A. Štrkalj, N. Pernet, J. L. Lado, C. Dorow, A. Lemaître, L. L. Gratiet, A. Harouri, I. Sagnes, S. Ravets, A. Amo, J. Bloch, and O. Zeitler, *Nat. Phys.* **16**, 832 (2020).
[28] F. A. An, E. J. Meier, and B. Gadway, *Phys. Rev. X* **8**, 031045 (2018).
[29] Y. Lahini, R. Pugatch, F. Pozzi, M. Sorel, R. Morandotti, N. Davidson, and Y. Silberberg, *Phys. Rev. Lett.* **103**, 013901 (2009).
[30] J. M. Zeuner, M. C. Rechtsman, Y. Plotnik, Y. Lumer, S. Nolte, M. S. Rudner, M. Segev, and A. Szameit, *Phys. Rev. Lett.* **115**, 040402 (2015).
[31] C. Poli, M. Bellec, U. Kuhl, F. Mortessagne, and H. Schomerus, *Nat. Commun.* **6**, 6710 (2015).
[32] P. Peng, W. Cao, C. Shen, W. Qu, J. Wen, L. Jiang, and Y. Xiao, *Nat. Phys.* **12**, 1139 (2016).
[33] H. Xu, D. Mason, L. Jiang, and J. G. E. Harris, *Nature (London)* **537**, 80 (2016).

- [34] S. Weimann, M. Kremer, Y. Plotnik, Y. Lumer, S. Nolte, K. G. Makris, M. Segev, M. C. Rechtsman, and A. Szameit, *Nat. Mater.* **16**, 433 (2017).
- [35] M. Pan, H. Zhao, P. Miao, S. Longhi, and L. Feng, *Nat. Commun.* **9**, 1308 (2018).
- [36] H. Zhou, C. Peng, Y. Yoon, C. W. Hsu, K. A. Nelson, L. Fu, J. D. Joannopoulos, M. Soljačić, and B. Zhen, *Science* **359**, 1009 (2018).
- [37] C. M. Bender and S. Boettcher, *Phys. Rev. Lett.* **80**, 5243 (1998).
- [38] Y. Ashida, Z. Gong, and M. Ueda, *Adv. Phys.* **69**, 249 (2020).
- [39] A. Mostafazadeh, *Int. J. Geom. Methods Mod. Phys.* **07**, 1191 (2010).
- [40] M. Znojil, *Phys. Rev. A* **100**, 032124 (2019).
- [41] Z. Gong, Y. Ashida, K. Kawabata, K. Takasan, S. Higashikawa, and M. Ueda, *Phys. Rev. X* **8**, 031079 (2018).
- [42] F. Song, S. Yao, and Z. Wang, *Phys. Rev. Lett.* **123**, 246801 (2019).
- [43] S. Yao and Z. Wang, *Phys. Rev. Lett.* **121**, 086803 (2018).
- [44] N. Okuma, K. Kawabata, K. Shiozaki, and M. Sato, *Phys. Rev. Lett.* **124**, 086801 (2020).
- [45] T. E. Lee, *Phys. Rev. Lett.* **116**, 133903 (2016).
- [46] D. Leykam, K. Y. Bliokh, C. Huang, Y. D. Chong, and F. Nori, *Phys. Rev. Lett.* **118**, 040401 (2017).
- [47] H. Shen, B. Zhen, and L. Fu, *Phys. Rev. Lett.* **120**, 146402 (2018).
- [48] F. K. Kunst, E. Edvardsson, J. C. Budich, and E. J. Bergholtz, *Phys. Rev. Lett.* **121**, 026808 (2018).
- [49] K. Yokomizo and S. Murakami, *Phys. Rev. Lett.* **123**, 066404 (2019).
- [50] D. S. Borgnia, A. J. Kruchkov, and R.-J. Slager, *Phys. Rev. Lett.* **124**, 056802 (2020).
- [51] N. Hatano and D. R. Nelson, *Phys. Rev. Lett.* **77**, 570 (1996).
- [52] P. W. Brouwer, P. G. Silvestrov, and C. W. J. Beenakker, *Phys. Rev. B* **56**, R4333(R) (1997).
- [53] A. F. Tzortzakakis, K. G. Makris, and E. N. Economou, *Phys. Rev. B* **101**, 014202 (2020).
- [54] Y. Huang and B. I. Shklovskii, *Phys. Rev. B* **101**, 014204 (2020).
- [55] K. Kawabata and S. Ryu, *Phys. Rev. Lett.* **126**, 166801 (2021).
- [56] X. Luo, T. Ohtsuki, and R. Shindou, *Phys. Rev. B* **104**, 104203 (2021).
- [57] X. Luo, Z. Xiao, K. Kawabata, T. Ohtsuki, and R. Shindou, *Phys. Rev. Res.* **4**, L022035 (2022).
- [58] X.-W. Luo and C. Zhang, [arXiv:1912.10652](https://arxiv.org/abs/1912.10652).
- [59] X. Cai, *Phys. Rev. B* **103**, 014201 (2021).
- [60] Y. Liu, Q. Zhou, and S. Chen, *Phys. Rev. B* **104**, 024201 (2021).
- [61] Y. Liu, X.-P. Jiang, J. Cao, and S. Chen, *Phys. Rev. B* **101**, 174205 (2020).
- [62] S. Longhi, *J. Phys. A* **47**, 165302 (2014).
- [63] C. Yuce, *Phys. Lett. A* **378**, 2024 (2014).
- [64] C. H. Liang, D. D. Scott, and Y. N. Joglekar, *Phys. Rev. A* **89**, 030102(R) (2014).
- [65] A. K. Harter, T. E. Lee, and Y. N. Joglekar, *Phys. Rev. A* **93**, 062101 (2016).
- [66] D.-W. Zhang, L.-Z. Tang, L.-J. Lang, H. Yan, and S.-L. Zhu, *Sci. China Phys. Mech. Astron.* **63**, 267062 (2020).
- [67] S. Longhi, *Phys. Rev. Lett.* **122**, 237601 (2019).
- [68] N. X. A. Rivolta, H. Benisty, and B. Maes, *Phys. Rev. A* **96**, 023864 (2017).
- [69] Q.-B. Zeng, Y.-B. Yang, and Y. Xu, *Phys. Rev. B* **101**, 020201(R) (2020).
- [70] S. Longhi, *Phys. Rev. B* **100**, 125157 (2019).
- [71] Q.-B. Zeng, S. Chen, and R. Lü, *Phys. Rev. A* **95**, 062118 (2017).
- [72] A. Jazaeri and I. I. Satija, *Phys. Rev. E* **63**, 036222 (2001).
- [73] S. Longhi, *Opt. Lett.* **44**, 1190 (2019).
- [74] Q.-B. Zeng and Y. Xu, *Phys. Rev. Res.* **2**, 033052 (2020).
- [75] T. Liu, S. Cheng, H. Guo, and G. Xianlong, *Phys. Rev. B* **103**, 104203 (2021).
- [76] H. Jiang, L.-J. Lang, C. Yang, S.-L. Zhu, and S. Chen, *Phys. Rev. B* **100**, 054301 (2019).
- [77] S. Longhi, *Opt. Lett.* **45**, 4036 (2020).
- [78] L. Z. Tang, G. Q. Zhang, L. F. Zhang, and D. W. Zhang, *Phys. Rev. A* **103**, 033325 (2021).
- [79] T. Liu, H. Guo, Y. Pu, and S. Longhi, *Phys. Rev. B* **102**, 024205 (2020).
- [80] X. Xia, K. Huang, S. Wang, and X. Li, *Phys. Rev. B* **105**, 014207 (2022).
- [81] Z. Xu, X. Xia, and S. Chen, *Sci. Chin. Phys. Mech. Astron.* **65**, 227211 (2022).
- [82] Y. Liu, Y. Wang, X.-J. Liu, Q. Zhou, and S. Chen, *Phys. Rev. B* **103**, 014203 (2021).
- [83] Y. Liu, Y. Wang, Z. Zheng, and S. Chen, *Phys. Rev. B* **103**, 134208 (2021).
- [84] X. Cai and S.-J. Jiang, *New J. Phys.* **24**, 113001 (2022).
- [85] A. Avila, *Acta Math.* **215**, 1 (2015).
- [86] Y.-C. Zhang and Y.-Y. Zhang, *Phys. Rev. B* **105**, 174206 (2022).
- [87] X. Cai, *Phys. Rev. B* **103**, 214202 (2021).
- [88] J. Schindler, A. Li, M. C. Zheng, F. M. Ellis, and T. Kottos, *Phys. Rev. A* **84**, 040101(R) (2011).
- [89] T. Hofmann, T. Helbig, C. H. Lee, M. Greiter, and R. Thomale, *Phys. Rev. Lett.* **122**, 247702 (2019).
- [90] As integer j changes from $-\infty$ to $+\infty$, values of $2\pi\beta j \bmod 2\pi$ are uniformly distributed in set $[0, 2\pi]$, due to the irrational nature of β . Thus, we can turn the summation into an integration.
- [91] https://en.wikipedia.org/wiki/Jensen's_formula.